A real-time energy management and speed controller for an electric vehicle powered by a hybrid energy storage system

Lijun Zhang, Xianming Ye, Xiaohua Xia, Farshad Barzegar

***Abstract*—A real-time unified speed control and power flow management system for an electric vehicle (EV) powered by a battery-supercapacitor hybrid energy storage system (HESS) is developed following a nonlinear control system technique. In view of the coupling between energy management and HESS sizing, a HESS sizing model is developed to optimally determine the size of HESS to serve an EV using the controller designed. The objectives of the controller are to track the set speed of the vehicle with globally exponential stability and to make use of the HESS wisely to reduce battery stress. The design provides compound controller by exploiting the physical origins of the vehicles' power demand. The controller and HESS sizing system designed are simulated on a standard urban dynamometer driving schedule and a recorded actual city driving cycle for a full-size EV to demonstrate their effectiveness.**

***Index Terms*—Electric vehicles, controller design, energy management, speed control, hybrid energy storage system.**

I. Introduction

Hybrid and pure electric vehicles (EVs) are being promoted globally today [1], [2]. Whereas the benefits of EVs are obvious, the bottleneck for their development is the energy storage system, which needs to provide power and energy throughout an EV's lifetime. For this purpose, supercapacitor and battery hybrid energy storage system (HESS) and its application in EVs have been brought into the sight of researchers [3]. This type of HESS combines the benefits of both battery and supercapacitor by using high energy density of the battery to provide energy support for the vehicle over a driving mission and high power density of the supercapacitor to satisfy peak power demands of the vehicle during transients and regenerative braking [4]. In such a way, the supercapacitor can protect the battery from fast charging/discharging and therefore extend the battery lifetime.

The HESS, however, brings about new challenges in four aspects, namely, topology design, DC-DC converter design, energy management, and optimal sizing of components. Three topologies namely passive, semi-passive, and fully active topologies were proposed and each with specific advantages and drawbacks discussed in [5]. Pertaining DC-DC converters, a tri-state bidirectional buck-boost converter was designed in [6], and a nonlinear controller for two converters used in fuel cell/supercapacitor hybrid EVs was proposed in [7], etc.

Energy management of the HESS for the EV's vibrant operating conditions is another challenging task, which aims to effectively split the vehicle power demand between batteries and supercapacitors for the purposes of reducing energy losses in the powertrain and alleviating power stress [8]. Energy management and control systems are usually required to fulfill this function. In particular, the aim of the power flow management for the battery-supercapacitor type HESS is to, taking advantages of the battery's high energy density and the supercapacitor's high power density characteristics, supply the slow varying power demand of the vehicle by the battery and the fast varying power demand by the supercapacitor. Usually, the batteries are referred to as the primary energy source because it provides the energy required to cover the driving range of the EV while supercapacitors support the battery when the vehicle needs high instant power or when the vehicle is regenerative braking, and are termed as the secondary energy source [7].

The energy management strategies reported in the literature can be broadly classified into three categories from a methodology perspective, namely, heuristic methods, filtration based methods, and optimization based methods. Heuristic methods include deterministic rule-based [9], [10] and fuzzy logic mechanism based [11], [12] ones. Inspired by frequency separation of the vehicle power demand, low pass filter (LPF) based energy management strategies are also investigated with the idea of assigning the low frequency slow varying power demand to batteries in battery/supercapacitor powered [13], [14] and battery/fuel cell powered vehicles [15].

The heuristic- and filtration-based methods are conceptually simple and easy to implement. However, they do not guarantee the optimal operation of the HESS. The optimization-based methods try to find the global optimal solution by means of solving an optimization problem formulated with one or more objectives [8]. These optimization problems are usually nonlinear and difficult to solve. Therefore, dynamic programming (DP) is commonly used [16], [17]. This method, however, suffers from a heavy requirement on computing resources and long computational time and only works offline. In terms of real-time applicability, the heuristic- and filtration-based methods can be implemented online while the optimization base methods usually require prior knowledge of the driving cycle and compute an offline solution. In recent studies, [18] tried to reduce the computational burden of DP by applying

All authors are with the Department of Electrical, Electronic and Computer Engineering, University of Pretoria, Pretoria 0002, South Africa. Emails: lijun.zhang@up.ac.za, xianming.ye@up.ac.za, xxia@up.ac.za, farshadbarzegar@gmail.com.

This research is supported by the National Research Foundation under grant number: 114141 and the University of Pretoria under grant number: A0Z785.

Pontryagin's maximum principle but still concluded that the results are not applicable in real-time.

Using meta-heuristic algorithms such as genetic algorithm [19], neural networks [20], particle swarm, and simulated annealing [21] to find sub-optimal solutions of the power split problem in real-time have also been reported. In particular, researchers have also tried to either divide the EV energy management problem into multilevels that deal with energy and power requirements at different layers to reduce complexity [22], [21] or formulate a simplified optimization problem and solve it by the Karush-Kuhn-Tucker (KKT) conditions method considering only battery power smoothing [20], or, both battery power smoothing and power loss reduction [8].

These results shown very promising results through simulations and experimental validations. One drawback, however, is that they all managed the power split according to the vehicle's power demand, either through measured motor current [11], [23] or power [12], [21] at the DC bus of the HESS and used this power information as an input to determine the best power split. Although vehicle speed was taken as an input in [20], the presented neural network energy management system requires extensive training data for an anticipated driving pattern. In other words, the energy management strategies developed so far mostly are using power demand of the vehicle calculated from a given driving cycle offline, or measured power demand of the vehicle at the DC bus of the HESS in real-time operation. The sources of the vehicle power demand, such as power required to accelerate, to overcome rolling resistance, gravitational drags, are not considered separately and thus their characteristics are not fully exploited for the purpose of energy management systems design.

The objective of this study is to design a real-time power split strategy taking into account different sources of the vehicle's power demand. The strategy is designed in such a way that it not only determines the power split for the HESS but also fulfills the speed control of the vehicle, and is referred to as a compound controller.

The advantages and benefits of the controller proposed are that it 1) provides a real-time energy management and speed controller of the vehicle based on Lyapunov's stability theory; 2) does not require prior knowledge of the vehicle's driving schedule; 3) uses physical insights into the vehicle power demand to facilitate power split in the HESS; 4) the designed power split has clear physical meanings and is easy to implement by field engineers without specialized training.

In particular, the battery is used to supply the power required by the vehicle to overcome resistances and aerodynamic drags, which varies gently, and supercapacitors are used to satisfy fluctuating power demands because of acceleration/deceleration and gravitational resistance.

This unified approach provides better performance by taking advantage of the EV's operating conditions and parameters. It also facilitates a better understanding of the power management requirement in EV applications. Moreover, the unified approach provides speed tracking ability to a set velocity profile, a feature that was not explored by the vehicle energy management studies. This added feature contributes positively towards the future development of self-driving EVs.

In addition, this study presents a HESS sizing strategy specifically developed for use together with the controller proposed taking into consideration of battery degradation, vehicle power demand, and mass of the HESS. In the literature, optimal HESS sizing is usually achieved by solving an optimization problem with the objectives including minimizing weight, cost, and battery degradation of the HESS depending on the energy management strategy employed. For instance, [13] presented a combined sizing and energy management strategy for HESS based on filter-based frequency separation of the vehicle's power demand. [9] reported a sizing method according to a rule-based power split strategy. A multi-objective sizing strategy taking into account state-of-health the battery based on a wavelet-transform-based energy management strategy was also reported in [24]. The sizing method developed in this study is largely based on the work presented in [9].

For the controller design purposes, the motion dynamics of the vehicle is modeled from first principles. The designed controller is simulated with a full sized EV, running through the urban dynamometer driving schedule (UDDS) developed by the US environmental protection agency, which represents city driving conditions and is often used for light duty vehicle testing [25], and a recorded actual city driving cycle. The results obtained are compared to the state-of-the-art real-time energy management results published in [9] and [8] to show its benefits.

The remainder of this paper is organized as follows. Section II presents the mathematical modeling of the EV. Section III presents the controller design. Section V gives simulation results and Section VI concludes this study.

II. EV MODELING

A. Motion dynamics

Motion dynamics of the EV running on a track can be derived from force analysis of the vehicle. From Newton's second law, one gets:

$$m\dot{v} = f_t - f_a - f_r, \tag{1}$$

where v in m/s is the vehicle speed. m is the mass of the vehicle in kg. f_t is the traction force provided by the driving motor in N, f_a is the aerodynamic drag and f_r consists of the rolling resistance and resistance caused by gravitational acceleration in N given by [26]:

$$f_a = \frac{1}{2}\rho_a C_d A_f v^2,$$
$$f_r = mg\mu\cos(\alpha) + mg\sin(\alpha),$$

where ρ_a is the air density in kg/m^3, C_d is the air drag coefficient and A_f is the frontal cross sectional area of the vehicle in m^2, μ is the rolling resistance coefficient, which depends on factors including road surface conditions, tire pressure and size, etc. g is the gravitational acceleration in m/s^2 and α is the slope of the road in rad.

B. Powertrain characteristics

The power required by a vehicle moving at speed v is

$$p_{ev} = f_t v = (f_a + f_r + m\dot{v})v. \tag{2}$$

This p_{ev} in W must be supplied by the HESS through the powertrain. With the focus of this paper being developing an effective controller, detailed modeling of the powertrain components is not performed. Instead, it is assumed that the battery, supercapacitor, and power electronic components can be simplified to have constant energy transmission/conversion efficiencies. As a result, (3) must be valid at all times in order to satisfy the power demand of the EV.

$$p_{ev} = \eta_d \left(\eta_{bat} p_{bat} + \eta_{sc} p_{sc}\right), \tag{3}$$

where η_d is the combined mechanical transmission efficiency and the efficiency of the electric motor represented by its efficiency map shown in Figure 2 (notice that the η_d will be greater than 1 when $p_{ev} < 0$). η_{sc} includes the supercapacitor discharging and DC-DC converter efficiencies when $p_{ec} > 0$, while it includes the supercapacitor charging and DC-DC converter efficiences otherwise. η_{bat} is the discharging efficiency of the battery. p_{bat} and p_{sc} are the discharging/charging powers of the battery and supercapacitor in W, respectively.

III. Controller design

A. Control objectives

The controller aims to regulate the speed of the vehicle and at the same time optimally manage power flows in the HESS. Therefore, the controller must be capable of tracking the desired speed of the vehicle while using the hybrid energy storage system in a way that reduces battery stress.

Therefore, the main objectives of the real-time compound controller are twofold: 1) speed control: ensuring good speed track performance of the EV and guaranteeing the global asymptotic stability of the speed tracking error; and 2) energy management: relieving battery stress and prolonging battery life by protecting the battery from abrupt power flows/currents.

B. Nonlinear controller design

A Lyapunov-based nonlinear controller is designed for the EV because of the nonlinearities involved in the EV dynamics (1). To achieve the first control objective, tracking of the set speed v_r, the speed tracking error is defined as $e = v_r - v$.

Achieving tight tracking of the set speed entails the regulation of the error e at zero. To this end, the dynamics of e has to be defined. Calculating the derivative of e leads to

$$\dot{e} = \dot{v}_r - \frac{f_t - f_a - f_r}{m}. \tag{4}$$

Combing (2)–(4), one gets

$$\dot{e} = \dot{v}_r - \frac{\eta_d(\eta_{bat} p_{bat} + \eta_{sc} p_{sc})}{mv} + \frac{\rho_a C_d A_f v^2}{2m} - g\mu\cos\alpha - g\sin\alpha. \tag{5}$$

To make e exponentially vanish amounts to enforce

$$\dot{e} = -ke, \tag{6}$$

where k is a positive design parameter.

Comparing (5) and (6), this study proposes the following control law:

$$\begin{cases} p_{bat} = \frac{mv}{\eta_d \eta_{bat}} \left(\frac{\rho_a C_d A_f}{2m} v_r^2 + g\mu\cos\alpha \right), \\ p_{sc} = \frac{mv}{\eta_d \eta_{sc}} \left(g\sin\alpha + \dot{v}_r \right). \end{cases} \tag{7}$$

The control law given in (7) is inspired by the physical operation of the vehicle and the characteristics of the HESS. To be specific, the vehicle requires a sharp power increase/decrease when accelerating/decelerating and moving up/down hills. Knowing that supercapacitors can be used to handle the sharp power flows to protect the battery, the control law allows the battery to supply power required by the vehicle to overcome the aerodynamic drag and rolling resistance, which vary smoothly, and the supercapacitor to supply power required for acceleration/deceleration and the gravitational resistance, which can change abruptly. In addition, the control law directs all regenerative braking power to the supercapacitor due to its fast charging capability [3]. The added benefit is that a semi-active configuration of the HESS can be used to reduce weight and costs of power converters.

***Remark** 1:* Firstly, the control law (7) is given in terms of the power flows. In the practical EV control, this can be translated into currents from the battery and supercapacitor by dividing their respective voltages. It then follows that the controller designed generates reference battery and supercapacitor currents, which should be tracked by a lower level DC-DC converter controllers associated with the HESS. Secondly, the control law (7) would fail in case $v = 0$ and $v_r > 0$. In this case, however, one could replace v in the control law by v_r and the controller will work because v will become nonzero after one sampling interval.

C. Stability analysis

***Proposition** 1:* Consider the nonlinear closed-loop error dynamics of the vehicle (5) and the control law given in (7). The speed tracking error is globally asymptotically stable.

Proof: The error dynamics of the speed tracking can be derived by substituting (7) into (5), which yields

$$\dot{e} = -\frac{\rho_a C_d A_f}{2m}(v_r + v)e.$$

Because $\frac{\rho_a C_d A_f}{2m}(v_r + v)$ is strictly positive everywhere except $v_r = v = 0$, which corresponds to $e = 0$. It follows that the error of the tracking vanishes to zero exponentially. Actually, one can choose a Lyapunov function

$$V = \frac{1}{2}e^2,$$

which is positive definite and radically unbounded. Then

$$\dot{V} = -\frac{\rho_a C_d A_f}{2m}(v_r + v)e^2$$

is negative definite. Therefore, the error system is globally exponentially stable. ■

IV. Optimal sizing of the HESS

The HESS sizing and energy management or control strategy development are highly coupled processes for EVs. Once an energy management system is developed, a HESS sizing method is indispensable to put the energy management system in action and vice versa. In the following, sizing of the HESS to work optimally with the controller designed is presented.

In the sizing process, one important target is to make sure that the battery used in the vehicle can endure a specified lifespan. In this regards, it is commonly accepted that the battery capacity loss must be within 20% after ten years of operation [9]. To take this into account in the sizing process, a battery degradation model is essential.

A. Battery degradation model

Several battery degradation models have been presented in the literature [27], [28]. The one that is most suitable for evaluating capacity loss of lithium-ion EV batteries was presented and experimentally validated in [28]. This model takes an exponential form as shown in (8) and is most commonly used in the EV community.

$$Q_{loss} = Be^{-E_a/RT}A_h^{\rho}, \tag{8}$$

where Q_{loss} is the percentage of battery capacity loss, B is the pre-exponential factor, E_a is the activation energy from Arrhenius law in J mol^{-1}, A_h is the Ah-throughput, T is the absolute temperature in K, and $R = 8.314$ J mol^{-1}K^{-1} is the gas constant. $\rho = 0.5$ is the power law factor. The rest parameters of the capacity loss model were empirically obtained from a large set of testing data. The E_a is related to current and can be calculated by

$$E_a = 31500 - 370.3C_{rate},$$

where C_{rate} is the current rate. The charge throughput is calculated by $A_h = N \times DoD \times C$, in which N is the cycle number, DoD is the depth-of-discharge and C is the full capacity of the battery in Ah.

This model was initially tested under four current rates, 1/2C, 2C, 6C and 10C, and was extended to general scenarios for current rates below 10C in [9], which resulted in

$$\ln B = ae^{-\lambda C_{rate}} + d = 1.226e^{-0.2797C_{rate}} + 9.263.$$

However, this model initially was not tested under nonuniform current profiles. Shen et al. [9] then extended this model for such cases and presented a statistical method to determine capacity loss under nonuniform current profiles using the following procedure.

Firstly, a histogram of the battery current rates is obtained. Then the DoD of the battery at each current rate is calculated as $DoD(k)$, where k denotes the k-th current rate.

Secondly, the battery capacity loss is determined by

$$Q_{loss} = \sum_k Q(k),$$

where $Q(k)$ is determined according to equation (8) by

$$Q(k) = B(C_{rate}(k))e^{-\left(\frac{E_a(C_{rate}(k))}{RT}\right)}A_h(DoD(k))^{\rho}.$$

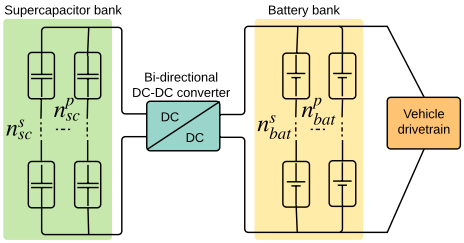

Fig. 1: Diagram of the HESS for sizing purposes

B. HESS sizing model

An optimal sizing model is given here with the objective to minimize the weight of the HESS while considering the limit on 20% battery capacity loss over a ten year period.

The HESS sizing is highly dependent on the topology of the HESS. The formulation given here is for a semi-active configuration, which suits the designed energy management system and speed controller. The HESS diagram for which the sizing problem is developed is shown in Figure 1.

The sizing problem is then formulated as minimizing the following objective function

$$f(n^s_{sc}, n^p_{sc}, n^s_{bat}, n^p_{bat}) = n^s_{sc}n^p_{sc}m^{cell}_{sc} + n^s_{bat}n^p_{bat}m^{cell}_{bat}, \tag{9}$$

subject to constraints defined in equations (10)-(17).

$$0.3n^s_{sc}v^{cell}_{sc} \geq V_{l,min}, \tag{10}$$
$$n^s_{sc}v^{cell}_{sc} \leq V_{l,max}, \tag{11}$$
$$V_{h,min} \leq n^s_{bat}v^{cell}_{bat} \leq V_{h,max}, \tag{12}$$
$$n^s_{sc}n^p_{sc}p^{cell}_{sc} \geq p_{ev,sc}, \tag{13}$$
$$n^s_{sc}n^p_{sc}p^{cell}_{sc} + n^s_{bat}n^p_{bat}p^{cell}_{bat} \geq p_{ev,max}, \tag{14}$$
$$n^s_{sc}n^p_{sc}e^{cell}_{sc} \geq e_{ev,sc} - e_{reg}, \tag{15}$$
$$n^s_{bat}n^p_{bat}e^{cell}_{bat} \geq e_{ev,bat}, \tag{16}$$
$$Q_{loss,10} \leq 0.2. \tag{17}$$

In the above formulation, subscripts bat, sc and ev denote variables associated with battery, supercapacitor and EV, respectively. The superscript $cell$ denotes variables for a cell of battery or supercapacitor, n denotes number of cells, and p and e represent power in W and energy in Wh, respectively. In addition, superscripts s and p denote numbers of cells connected in series and parallel, respectively (see Figure 1). $V_{l,min}$ and $V_{l,max}$ are the min and max voltages required by the DC/DC converter at the low voltage side in V. $V_{h,min}$ and $V_{h,max}$ are the lower and upper limits of the voltage at the high voltage side in V.

The constraints (10)-(12) ensure the proper working conditions for the DC/DC converter is maintained. (13) states that the power supply of the supercapacitor bank must meet the maximum power demand of the vehicle allocated to supercapacitors. (14) makes sure that the total power supply of the HESS can meet the maximum power demand of the EV. (15)-(16) ensure that the energy required by the EV is satisfied by the HESS, where e_{reg} denotes the regenerative energy. Lastly, (17) limits the battery capacity loss over ten years to be less than or equal to 20%.

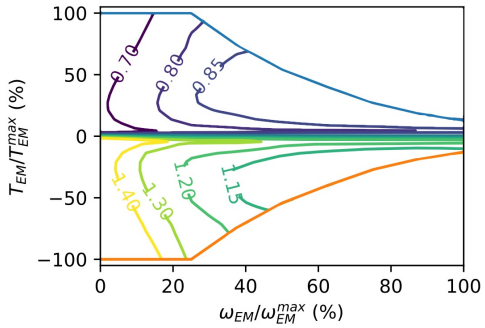

Fig. 2: Electric motor efficiency map

TABLE I: parameters of battery and supercapacitor cells

Parameter	Battery	Supercapacitor
Nominal voltage (V)	3.3	2.7
Nominal capacity (Ah)	44	0.75
Rated capacitance (F)	–	2000
Internal resistance (mΩ)	3.6	0.35
Energy storage (Wh)	140	2.03
Weight (kg)	0.9	0.36
Max. continuous discharge current (A)	50	120
Max. pulse discharge current (A)	100	1600
discharging/charging efficiency	0.95	0.99

TABLE II: EV related parameters

Parameter	Full size EV
vehicle mass (kg)	1500
vehicle frontal area (m^2)	2.35
transmission efficiency	0.98
gravitational acceleration (m/s^2)	9.8
air density (kg/m^3)	1.02
air drag coefficient	0.3
rolling resistance coefficient	0.01

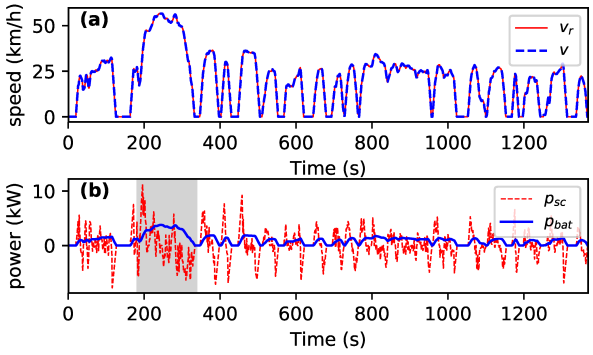

Fig. 3: UDDS cycle simulation results

V. Simulations

Simulation results are presented to demonstrate the effectiveness of the proposed control strategy and HESS sizing model. In particular, simulations are done for two scenarios for a full sized EV. The first one is over the UDDS cycle. The results of this simulation are firstly compared to a benchmark study [9], which presented a real-time power split and a HESS sizing strategy. To further compare the results to the latest real-time power split strategies, the results are also compared to those obtained in [8] in order to verify the benefits of the compound controller with respect to the state-of-the-art literature. The second case is for the same EV driving through a recorded city route to investigate the influences of an uneven road and a more dynamic driving style than the UDDS cycle. Additionally, a simulated acceleration test was done to reveal the effects of vehicle acceleration on the power flows.

The parameters of the HESS components are given in Table I and those of the EV are given in Table II. The voltage limits at the low voltage and high voltage sides of the DC-DC converter used are $V_{l,min} = 50$ V, $V_{l,max} = 430$ V, $V_{h,min} = 150$ V and $V_{h,max} = 750$ V according the specifications of a Brusa bidirectional DC-DC converter.

The motor efficiency map that is used to determine η_d is given in Figure 2, in which the speed and torque of the motor are normalized with respect to their maximum values.

A. The UDDS test

The effectiveness of the designed controller and HESS sizing model is firstly tested by means of simulations of a full-sized EV running through the UDDS [25]. The velocity tracking performance of the EV, together with the power profiles of the battery and supercapacitor over one UDDS cycle are shown in Figure 3.

Assuming the driver of the vehicle accomplishes six UDDS cycles per day and the maximum power demand of the EV is $p_{ev,max} = 80$ kW, the corresponding energy and power requirements for the battery and supercapacitor, *i.e.,* $e_{ev,bat}$, $e_{ev,sc}$, e_{reg} and $p_{ev,sc}$, in the HESS are determined. These values are then used to solve the HESS sizing problem by a genetic algorithm with a population size of 200, which results in a HESS comprising one string of 57 battery cells in series and three strings of 73 supercapacitor cells in series to optimally serve the vehicle.

Figure 3 shows that, as expected, the high-frequency power demand of the vehicle is supplied by the supercapacitor and low-frequency power is provided by the battery in the HESS. It can also be observed that the supercapacitor power in Figure 3 is used to provide/absorb power requirement/generation of the vehicle when accelerating/decelerating. For example, between 180 and 260 seconds, the vehicle is accelerating, which required a sharp increase in power supplied by the supercapacitor bank. After the daily driving mission, the state-of-charge of the supercapacitor is 61.9%. The UDDS simulation results following the compound controller presented in this study and those reported in [9] are compared in Table III. This table depicts that the control strategy in this study uses fewer batteries and more supercapacitors. This is because the majority of the high-frequency power requirement of the EV is supplied by the supercapacitor pack in the proposed control method while the heuristic method adopted in [9] allocates a relatively small fraction of high-frequency power demand to the supercapacitor bank.

As a result, the HESS sized in this study decreased the number of battery cells by 62.5% and increased the number

of supercapacitor cells by 204.2% in comparison to the sizing result in [9]. The mass and cost of the HESS also reduced by 20.0% and 2.7%, respectively. The decrease in the cost of the HESS is not significant at the current market price. However, the mass reduction of the HESS is noticeable which contributes to lowering the energy consumption of the EV. Regarding battery capacity loss, [9] achieved 15.9% over ten years for 152 battery cells. In comparison, this study achieved 3.4% (a 78.9% decrease) battery capacity loss over the same time period with noticeably fewer cells.

Although the parameters of the EV, the battery cells, supercapacitor cells, and the driving cycle used in the simulation are all the same, it is noticed that the sizing results of this study and those of [9] are fundamentally different because of the power management strategies employed. In this study, a nonlinear control based approach is presented, which resulted in a larger supercapacitor bank and a smaller battery bank.

In other words, the difference between the sizing results is mainly because of the control strategy. The large number of battery cells in the results reported in [9] is optimal for the heuristic strategy developed therein, while it is almost three times oversized for the controller designed in this study. The contrary is true for the supercapacitor sizing results. Taking advantage of the controller designed in this study, which protects the battery from abrupt discharges, fewer battery cells can be used while still satisfying the capacity loss limit over the lifespan of the EV. The other benefits of the control strategy and the corresponding HESS are the reduced cost of the HESS and even prolonged battery life as shown in Table III. To demonstrate the effectiveness of the proposed method, we also compared its results to other two categories of methods reported in the literature, *i.e.* the LPF method [13], and the DP optimization based method [29], which are the most popular methods used for the sizing and energy management of EVs. It can be seen that the results of the LPF method depends on the time constant τ (two sets of results are provided in the table). Nonetheless, the proposed method is able to provide favorable results.

The results obtained are also compared with those published in [8], in which the peak, average and average rate of change (defined by $ARC = \frac{1}{N}\sum_{n=2}^{N}|\frac{i_b - i_{b,pre}}{\Delta t}|$, where i_b and $I_{b,pre}$ are the current and previous battery current, respectively, and Δt is the sampling interval) of battery current are used to evaluate the effectiveness of battery power smoothing. With the same settings, it was found that the peak battery current resulted by the controller designed is 224 A, slightly less than rule-based power split strategy (228.1 A) and is higher than that obtained by the KKT based method (30.7-30.9 A) reported in [8]. However, the average current achieved by the designed controller is 5.3 A, much lower than 24.5 A of the rule-based method and 24.5-24.6 A obtained in [8]. Moreover, the ARC of battery current resulted by the designed controller is also comparable with that reported by [8], both achieving about 0.06 A/s in comparison to 7.16 A/s from a rule-based method. Therefore, the compound controller designed in this study is able to reduce battery stress more effectively because of the low average and ARC battery currents.

B. Actual city road test

The UDDS test is however over a flat route. In order to demonstrate the effectiveness of the designed controller on an actual uneven city road, a driving cycle recorded is used to simulate the performance of the control strategy. The speed of the vehicle and the elevation of the road are recorded along a city route shown in Figure 4.

The results of the simulation are shown in Figure 5, in which the subplots (a), (b), (c) and (e) show the speed tracking of the EV, the power profiles of battery and supercapacitor banks, the relative elevation of the route, respectively. From these subplots, it can be seen that the supercapacitor supplies/absorbs the fast-changing power flows of the vehicle because of acceleration/deceleration and gravitational acceleration. Additionally, subplot (b) depicts that the battery bank is continuously discharging and the supercapacitor gets charged during the vehicle's braking period, which is influenced by both the vehicle's speed profile and the slope of the route.

Unlike the UDDS test, this actual city test is over an uneven road, of which the slope influences the resulting power profiles. The recorded speed profile of the vehicle is also noticeably more dynamic than that of the UDDS cycle. To better understand what is the main cause of the fluctuations in the EV's power demand, p_{ev} is decomposed into four components as follows:

$$p_{ev} = p_{aero} + p_{grav} + p_{roll} + p_{acc},$$

where $p_{areo} = f_a v$ and $p_{grav} = mgv\sin(\alpha)$ are the power demands due to aerodynamic drag and gravitational force, respectively. $p_{roll} = mgv\mu\cos(\alpha)$ and $p_{acc} = m\dot{v}v$ are the power demands caused by the rolling resistance and the vehicle's acceleration/deceleration, respectively.

Because the controller designed in (7) assigns p_{acc} and p_{grav} to the supercapacitor bank and p_{roll} and p_{aero} to the battery bank, these powers are plotted in the subplots (d) and (e) together with p_{bat} and p_{sc}, respectively. The subplot (d) of Figure 5 reveals that at slow speed, rolling resistance is the main cause of the battery power output while the aerodynamic drag also becomes significant at high speed. From subplot (e) of Figure 5, it is also clear that the fast fluctuation in the power profile of the supercapacitor bank is mainly caused by p_{acc} as a result of the vehicle's change in speed whereas the slope of the road does not have significant impact in this aspect. A zoom-in plot from 600 s to 650 s is provided for a clearer view of this fact. In addition, the accelerations also contribute largely to the peak powers of the supercapacitor bank, for instance around 200 s. Around 650 s, the vehicle experiences a sharp acceleration while driving on an inclined road, which results in the highest supercapacitor power over the route. By

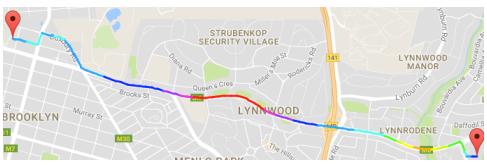

Fig. 4: Map of the recorded route

TABLE III: Results comparisons with existing literature

Parameters	Benchmark [9]	This study	**Comparison**	LPF $\tau = 10$ [13]	LPF $\tau = 1$ [13]	DP inspired [29]
no. of battery cells	152	57	$\downarrow$ 62.5%	58	61	61
no. of supercapacitor cells	72	219	$\uparrow$ 204.2%	219	216	216
HESS weight (kg)	162.7	130.1	$\downarrow$ 20.0%	131	132.7	132.7
HESS cost (USD)	14578	14181	$\downarrow$ 2.7%	14181	14267	14267
$Q_{loss,10}$ (%)	15.9	3.4	$\downarrow$ 78.9%	1.3	5.2	6.3

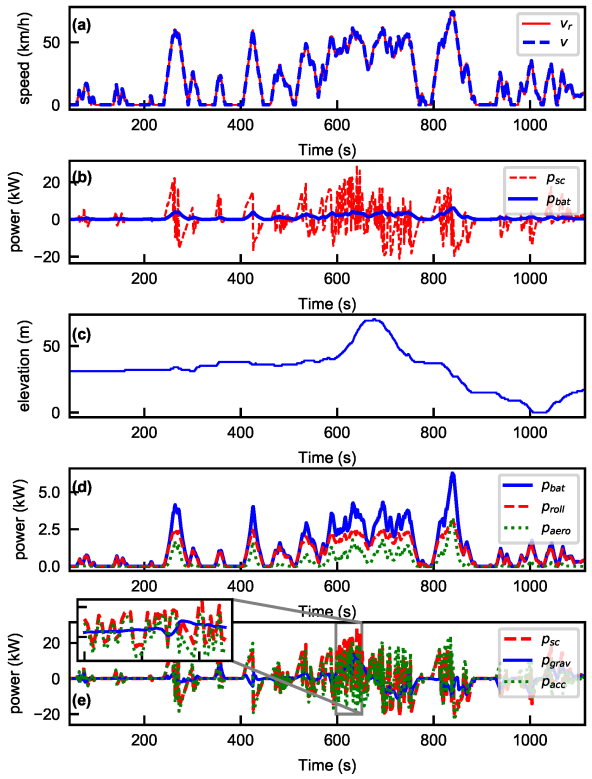

Fig. 5: Results of an actual city driving cycle

contrast, the vehicle had another fast acceleration around 850 s when it is driving downhill. In this case, the power demand from the supercapacitor was not as high as that around 650 s because the gravity aided the vehicle's acceleration. This suggests that the supercapacitor power is highly affected by driver behavior and road conditions, especially the former. An experienced driver who drives the vehicle smoothly will need less power from supercapacitor than a driver who drives more aggressively.

Again assuming the driver repeats the recorded cycle six times a day, the HESS sizing was done. The resulting HESS requires 57 battery cells and three strings of 73 supercapacitor cells each, which is the same as the sizing result for the UDDS. Since this test is done over a slightly shorter distance (6.3 km in comparison to 7.5 km of the UDDS), the ten-year battery capacity loss is decreased slightly from 3.4% of the UDDS test to 3.3%. In this case, the state-of-charge of supercapacitor at the end of the day is 30%.

TABLE IV: Power fluctuation indicators

Indicators	UDDS	City test	Acc. test 1	Acc. test 2
$std(\frac{dp_{sc}}{dt})$	1.13	5.59	0.88	0.52
$std(\frac{dp_{bat}}{dt})$	0.07	0.13	0.08	0.06
$std(p_{sc})$	2.38	6.87	3.54	2.77
$std(p_{bat})$	0.87	1.32	1.82	1.58

C. Effectiveness of energy management

Figs. 3 and 5 show that the battery power is smoothened effectively by the supercapacitor for both the UDDS test and an actual road test. Besides, the HESS sizing model presented in Section IV selects optimal components for the HESS.

To quantify the effect of smoothing battery power profile by the designed strategy, the standard deviation of the battery and supercapacitor power flows, $std(p_{bat})$ and $std(p_{sc})$, are used to describe the magnitude fluctuation in these power flows and the standard deviation of the rate of changes of these two powers, $std(\frac{dp_{bat}}{dt})$ and $std(\frac{dp_{bat}}{dt})$ are used to capture their variation over time. These indicators are given in Table IV, which demonstrates that both magnitude change and variation over time of battery power is significantly slower than those of the supercapacitor power with the designed controller.

The last two columns in Table IV are provided to demonstrate the effect of vehicle acceleration on the power flows. In particular, two simulations (Acc. test 1 and Acc. test 2) were carried out. In the first one, the vehicle accelerates from standstill with $a = 0.3$ m/s^2 to 60 km/h, then decelerates at $a = -0.3$ m/s^2 to standstill. In Acc. test 2, the acceleration was increased to $0.5/-0.5$ m/s^2. When comparing Acc. test 2 to Acc. test 1, the variation of supercapacitor power is significant while that of the battery is not. Sensitivity of the defined performance indicators with respect to the acceleration change, $\frac{\Delta std(\frac{dp_{sc}}{dt})}{\Delta a} = 3.85$ and $\frac{\Delta std(p_{sc})}{\Delta a} = 1.78$ while these values for battery power are 1.19 and 0.09, respectively.

D. Closed-loop speed tracking performance

To validate the effectiveness of the speed controller to fulfill the second design objective stated in Section III, it is tested under measurement noises and modeling uncertainties. In particular, the controller requires feedback measurement of the vehicle's velocity and the slope of the road. Although, the speed of the vehicle can be measured with high accuracy [30] and the road slope can also be measured with an error band of less than 2% in real-time [31], these inevitably bring in inaccuracies. Additionally, the vehicle model is also limited by its accuracy due to some unmodeled dynamics, such as the simplifications of the rolling resistance model because of neglected time varying road surface and tire conditions.

Therefore, the robustness of the speed controller designed against these possible disturbances is investigated.

Considering the worst case with a random 5% measurement noise in the road slope together with a 5% error in the speed measurement due to the combined effect of measurement noise and modeling inaccuracy, simulations are done for the UDDS cycle and the recorded city road driving cycle. 20 runs are carried out for each of these cycles and the worst speed tracking results for each of them are analyzed. It is found that the maximum average speed tracking error is around 0.03 m/s (0.11 km/h). Thus, the controller is able to track the set speed of the vehicle with a negligible error in the presence of measurement noises and modeling uncertainties.

VI. Conclusion

A real-time compound controller is designed for the energy management and speed control of electric vehicles powered by a battery/supercapacitor hybrid energy storage system. The controller is able to smooth battery power effectively to prolong its lifetime for energy management, and is theoretically proved to be globally stable for speed control with feedback measurements on vehicle speed and road slope. Simulation results obtained from a simulated UDDS cycle and a recorded city test cycle show that it achieves less battery power fluctuation when compared to two existing studies and is able to follow the desired speed profile of the vehicle with minimum deviation when measurement noise and modeling uncertainties are taken into account. A sizing model is also presented to determine the numbers of battery and supercapacitor cells required to power the vehicle. The controller designed is for urban driving conditions, in future, an extension of the results for application in mountainous areas will be investigated by tackling the difficulties associated with road slope measurement and supercapacitor over-sizing due to consecutive up- or down-hills.

References

[1] C. M. Martinez, X. Hu, D. Cao, E. Velenis, B. Gao, and M. Wellers, "Energy management in plug-in hybrid electric vehicles: Recent progress and a connected vehicles perspective," *IEEE Transactions on Vehicular Technology*, vol. 66, no. 6, pp. 4534–4549, 2017.

[2] M. Bayati, M. Abedi, G. B. Gharehpetian, and M. Farahmandrad, "Short-term interaction between electric vehicles and microgrid in decentralized vehicle-to-grid control methods," *Protection and Control of Modern Power Systems*, vol. 4, no. 4, pp. 42–52, 2019.

[3] A. F. Burke and B. A. F. Burke, "Batteries and Ultracapacitors for Electric, Hybrid, and Fuel Cell Vehicles," *Proceedings of the IEEE*, vol. 95, no. 4, pp. 806–820, 2007.

[4] A. Khaligh, S. S. Member, Z. Li, S. S. Member, and Zhihao Li, "Battery, Ultracapacitor, Fuel Cell, and Hybrid Energy Storage Systems for Electric, Hybrid Electric, Fuel Cell, and Plug-In Hybrid Electric Vehicles: State of the Art," *IEEE Transactions on Vehicular Technology*, vol. 59, no. 6, pp. 2806–2814, 2010.

[5] R. Xiong, H. Chen, C. Wang, and F. Sun, "Towards a smarter hybrid energy storage system based on battery and ultracapacitor - A critical review on topology and energy management," *Journal of Cleaner Production*, vol. 202, pp. 1228 – 1240, 2018.

[6] G. R. Broday, C. B. Nascimento, E. A. Jr, L. A. C. Lopes, E. Agostini, and L. A. C. Lopes, "A Tri-State Bidirectional Buck-Boost Converter for a Battery/Supercapacitor Hybrid Energy Storage System in Electric Vehicle Applications," in *2015 IEEE Vehicle Power and Propulsion Conference (VPPC)*, Montréal, Canada, 2015, pp. 1–6.

[7] H. E. Fadil, F. Giri, S. Member, J. M. Guerrero, S. Member, and A. Tahri, "Modeling and Nonlinear Control of a Fuel Cell/Supercapacitor Hybrid Energy Storage System for Electric Vehicles," *IEEE Transactions on Vehicular Technology*, vol. 63, no. 7, pp. 3011–3018, 2014.

[8] X. Lu, Y. Chen, M. Fu, and H. Wang, "Multi-objective optimization-based real-time control strategy for battery/ultracapacitor hybrid energy management systems," *IEEE Access*, vol. 7, pp. 11 640–11 650, 2019.

[9] J. Shen, S. Dusmez, S. S. Member, A. Khaligh, and S. S. Member, "Optimization of Sizing and Battery Cycle Life in Battery/Ultracapacitor Hybrid Energy Storage Systems for Electric Vehicle Applications," *IEEE Transactions on Industrial Informatics*, vol. 10, no. 4, pp. 2112–2121, 2014.

[10] Y. Li, X. Huang, D. Liu, M. Wang, and J. Xu, "Hybrid energy storage system and energy distribution strategy for four-wheel independent-drive electric vehicles," *Journal of Cleaner Production*, vol. 220, pp. 756–770, 2019.

[11] M. Sellali, S. Abdeddaim, A. Betka, A. Djerdir, S. Drid, and M. Tiar, "Fuzzy-Super twisting control implementation of battery/super capacitor for electric vehicles," *ISA Transactions*, no. xxxx, 2019.

[12] J. P. F. Trovao, M. A. Roux, E. Menard, and M. R. Dubois, "Energy- and power-split management of dual energy storage system for a three-wheel electric vehicle," *IEEE Transactions on Vehicular Technology*, vol. 66, no. 7, pp. 5540–5550, 2017.

[13] R. E. Araújo, R. de Castro, C. Pinto, P. Melo, D. Freitas, R. D. Castro, C. Pinto, S. Member, P. Melo, S. Member, and D. Freitas, "Combined Sizing and Energy Management in EVs With Batteries and Supercapacitors," *IEEE Transactions on Vehicular Technology*, vol. 63, no. 7, pp. 3062–3076, 2014.

[14] Q. Zhang, W. Deng, and G. Li, "Stochastic Control of Predictive Power Management for Battery/Supercapacitor Hybrid Energy Storage Systems of Electric Vehicles," *IEEE Transactions on Industrial Informatics*, vol. 14, no. 7, pp. 3023–3030, 2018.

[15] J. Snoussi, S. B. Elghali, M. Benbouzid, and M. F. Mimouni, "Optimal sizing of energy storage systems using frequency-separation-based energy management for fuel cell hybrid electric vehicles," *IEEE Transactions on Vehicular Technology*, vol. 67, no. 10, pp. 9337–9346, 2018.

[16] Z. Song, H. Hofmann, J. Li, X. Han, and M. Ouyang, "Optimization for a hybrid energy storage system in electric vehicles using dynamic programing approach," *Applied Energy*, vol. 139, no. Dc, pp. 151–162, 2015.

[17] H. Jiang, L. Xu, J. Li, Z. Hu, and M. Ouyang, "Energy Management and Component Sizing for a Fuel Cell/Battery/Supercapacitor Hybrid Powertrain based on Two-Dimensional Optimization Algorithms," *Energy*, vol. 177, pp. 386–396, 2019.

[18] S. Uebel, N. Murgovski, C. Tempelhahn, B. Bernard, and B. Baker, "Optimal Energy Management and Velocity Control of Hybrid Electric Vehicles," *IEEE Transactions on Vehicular Technology*, vol. 67, no. 1, pp. 327–337, 2018.

[19] M. Wieczorek and M. Lewandowski, "A mathematical representation of an energy management strategy for hybrid energy storage system in electric vehicle and real time optimization using a genetic algorithm," *Applied Energy*, vol. 192, pp. 222–233, 2017.

[20] J. Shen and A. Khaligh, "Design and Real-Time Controller Implementation for a Battery-Ultracapacitor Hybrid Energy Storage System," *IEEE Transactions on Industrial Informatics*, vol. 12, no. 5, pp. 1910–1918, 2016.

[21] F. Machado, J. P. F. Trovão, and C. H. Antunes, "Effectiveness of supercapacitors in pure electric vehicles using a hybrid metaheuristic approach," *IEEE Transactions on Vehicular Technology*, vol. 65, no. 1, pp. 29–36, 2016.

[22] J. P. F. Trovão, V. D. Santos, C. H. Antunes, P. G. Pereirinha, and H. M. Jorge, "A Real-Time Energy Management Architecture for Multisource Electric Vehicles," *IEEE Transactions on Industrial Electronics*, vol. 62, no. 5, pp. 3223–3233, 2015.

[23] C. Zheng, W. Li, and Q. Liang, "An Energy Management Strategy of Hybrid Energy Storage Systems for Electric Vehicle Applications," *IEEE Transactions on Sustainable Energy*, vol. 9, no. 4, pp. 1880–1888, 2018.

[24] L. Zhang, X. Hu, Z. Wang, F. Sun, J. Deng, and D. G. Dorrell, "Multiobjective Optimal Sizing of Hybrid Energy Storage System for Electric Vehicles," *IEEE Transactions on Vehicular Technology*, vol. 67, no. 2, pp. 1027–1035, 2018.

[25] T. J. Barlow, S. Latham, I. S. Mccrae, and P. G. Boulter, "A reference book of driving cycles for use in the measurement of road vehicle emissions," *TRL Published Project Report*, p. 280, 2009.

[26] M.-E. E. Choi, J.-S. S. Lee, and S.-W. W. Seo, "Real-Time Optimization for Power Management Systems of a Battery/Supercapacitor Hybrid

Energy Storage System in Electric Vehicles," *IEEE Transactions on Vehicular Technology*, vol. 63, no. 8, pp. 3600–3611, 2014.

[27] Y. Gao, J. Jiang, C. Zhang, W. Zhang, Z. Ma, and Y. Jiang, "Lithium-ion battery aging mechanisms and life model under different charging stresses," *Journal of Power Sources*, vol. 356, pp. 103–114, 2017.

[28] J. Wang, P. Liu, J. Hicks-Garner, E. Sherman, S. Soukiazian, M. Verbrugge, H. Tataria, J. Musser, and P. Finamore, "Cycle-life model for graphite-LiFePO4 cells," *Journal of Power Sources*, vol. 196, no. 8, pp. 3942–3948, 2011.

[29] Z. Song, J. Li, J. Hou, H. Hofmann, and M. Ouyang, "The battery-supercapacitor hybrid energy storage system in electric vehicle applications: A case study," *Energy*, vol. 154, pp. 433–441, 2018.

[30] W. J. Fleming, "Overview of Automotive Sensors," *IEEE Sensors Journal*, vol. 1, no. 4, pp. 296–308, 2001.

[31] K. Jo, J. Kim, and M. Sunwoo, "Real-time road-slope estimation based on integration of onboard sensors with GPS using an IMMPDA filter," *IEEE Transactions on Intelligent Transportation Systems*, vol. 14, no. 4, pp. 1718–1732, 2013.